Catalysis Today 141 (2009) 220–224

Contents lists available at ScienceDirect

Catalysis Today

journal homepage: www.elsevier.com/locate/cattod

Photocatalytic activity of iron doped nanocrystalline titania for the oxidative degradation of 2,4,6-trichlorophenol

Periyasami Vijayan, Chinnathambi Mahendiran, Chinnathambi Suresh, Kannan Shanthi *

Department of Chemistry, Anna University, Chennai 600025, India

ARTICLE INFO

Article history:
Available online 18 June 2008

Keywords:
Photocatalysis
Nanocrystalline titania
UV-Vis DRS
Trichlorophenol

ABSTRACT

Pure and iron doped (0.3, 0.5, 0.7 and 1 wt.%) nanocrystalline TiO_2 have been synthesized by combining sol–gel technique with hydrothermal treatment. The resulting nanocrystals were characterized by X-ray diffraction (XRD), UV–visible diffused reflectance spectroscopy (UV–vis DRS), Electron paramagnetic resonance (EPR) spectroscopy and Transmission electron microscope (TEM) techniques. UV–vis DRS results showed that iron doping caused significant absorption shift towards visible region compared to Degussa P-25 and pure TiO_2. EPR spectra showed the presence of iron +3 oxidation state in TiO_2. From TEM image, it is obvious that the particle size is ranging from 10 to 30 nm. The photocatalytic activity of synthesized samples was investigated for the oxidative degradation of 2,4,6-trichlorophenol (2,4,6-TCP) in aqueous suspension. The photocatalytic activity of TiO_2 doped with 0.5 wt.% Fe exceeded those of non-doped commercial and synthesized pure TiO_2.

1. Introduction

The presence of harmful organic pollutants in wastewater effluents causes serious environmental problems. Purification of contaminated water is one of the most interesting challenges in catalysis today. In particular, with respect to the environmental protection issues, halogenated chemicals are difficult to decompose completely to CO_2, H_2O, and HCl by biological treatment, adsorption technology; air stripping and incineration. The stability of C–Cl bond in hydrocarbons is responsible for their toxicity and persistence in the biological environment [1]. Therefore, the current trend in treatment has moved from phase transfer to destruction of pollutants such as advanced oxidation processes (AOPs). Photocatalytic oxidation of water borne environmental contaminations by semiconductor powders irradiated with solar or UV light is a comparatively novel method for the destruction of toxic chemicals in water [2]. In most cases, the most effective materials for photocatalytic applications are nanosized semiconductor oxides. Among various oxide semiconductor photo catalysts, TiO_2 has been proven to be the most suitable photocatalyst for widespread environmental applications [3]. However, the use of TiO_2 as photocatalyst is mainly limited due to recombination of the generated photo-holes and photoelectrons. Considerable efforts have been made to dope TiO_2 with some transition and noble metals to improve the separation characteristics and hence photo-efficiency. Recently, researchers have demonstrated that the addition of certain metals such as platinum, palladium, gold, and some semiconductors can effectively enhance the degradation efficiency of photocatalytic reaction [4,5]. A few attempts have been made to employ transition metals doped TiO_2 as catalysts for the degradation of chlorophenols [6,7]. Degradation of 2,4,6-TCP in aqueous suspension has been carried out using Ag as the dopant ion in titania [6]. 2,4,6-TCP has been subjected to degradation by sequential photochemical and biological method using UV/TiO_2/H_2O_2 system [8]. Heterogeneous photocatalytic oxidation of aqueous solutions of 2,4,6-TCP using ultraviolet radiation, O_2 and TiO_2 in a pilot scale co-current downflow contactor reactor (CDCR) has been examined by mike Winterbottom and co-workers [9]. Lanthanum has been used as the dopant ion on ZnO semiconductor for the degradation 2,4,6-TCP in aqueous suspension and they found that the relative photonic efficiency and Photocatalytic activity of doped ZnO is more than the pure ZnO and pure TiO_2 [10].

Despite many modifications, TiO_2 suffer from major draw back due to its very low surface area. This can be overcome by preparing TiO_2 in nanoscale. Particle in nanoscale have more specific surface area which can enhance the rate of reaction. Sol–gel method is extensively utilized for the preparation of nanoarchitectured metallic oxides, in particular when it is desired to incorporate other metallic ions in the gels [11]. By controlling hydrothermal temperature and duration of hydrothermal treatment, one can synthesize the materials with required particle size. Hydrothermal

* Corresponding author. Tel.: +91 44 22203158.
E-mail address: kshanthiramesh@yahoo.com (K. Shanthi).

0920-5861/$ – see front matter © 2008 Published by Elsevier B.V.
doi:10.1016/j.cattod.2008.04.016

treatment is an environmentally benign process since it is done in a closed system [12]. Hence, catalysts synthesized by a novel route of combination of these two methods will be the opt one for the effective and complete mineralization of 2,4,6-trichlorophenol. In this work, highly photoactive iron doped nanocrystalline TiO_2 was prepared using sol–gel followed by hydrothermal methods and tested for the photocatalytic oxidative degradation of 2,4,6-trichlorophenol.

2. Experimental

2.1. Preparation of TiO_2 and Fe–TiO_2 nanoparticles

TiO_2 nanoparticles were synthesized by hydrolyzing titanium tetra isopropoxide (TTIP) (Lancaster, +97%) in a mixture of anhydrous ethanol and water. In a typical synthesis, 9 ml of TTIP is mixed with 41 ml of anhydrous ethanol (A). 50 ml of water mixed with 50 ml of anhydrous ethanol (B). Solution A is added drop wise to solution B with constant and vigorous stirring for 2 h. Required amount of ferric nitrate ($Fe(NO_3)_3{\cdot}9H_2O$) was added. Hydrolysis and condensation were conducted at room temperature using 1 M sulphuric acid and stirred for 2 h. Then it was undergone ageing for 12 h. The gel was transferred to autoclave and tightly closed. The mixture was subjected to hydrothermal treatment at 353 K for 24 h the solid residue was recovered by filtration after it was washed thoroughly with water and ethanol mixture and dried in an oven at 373 K overnight and calcined at 773 K.

2.2. Characterization of TiO_2 nanoparticles

The TiO_2 samples were characterized by powder X-ray diffraction (XRD) with Phillips X'pert PANalytical model using Cu-Kα radiation. XRD pattern were obtained for 20–80° (2θ) by step scanning with a step size of 0.02θ. UV–vis diffused reflectance spectra of the samples were recorded with Shimadzu UV 2450 model using $BaSO_4$ white plate as reference. The electron paramagnetic resonance (EPR) spectra of iron doped samples were recorded on Varian E-112 spectrometer operated at X-band frequency of 9.2 GHz at room temperature in solid state itself. Transmission electron micrographs (TEM) of catalysts were taken by JEOL TEM instrument.

2.3. Photocatalytic reactor set-up

Photocatalytic degradation was performed in a slurry batch reactor. The irradiation was carried out using 8 × 8 W low pressure mercury lamp built into lamp housing with polished anodized aluminium reflectors and placed 6.5 cm away from the reactor. The lamps emit predominantly UV radiation at a wavelength of 365 nm. 100 ml of 50 ppm 2,4,6-trichlorophenol was taken and stirred for 30 min to attain adsorption–desorption equilibrium and then irradiated. The sample was collected at the interval of every 30 min and filtered through 0.2 μm filter. The filtered samples were analyzed by total organic carbon analyzer (TOC, Shimadzu V_{CPN} model) and high performance liquid chromatography (HPLC). Concentration of 2,4,6-trichlorophenol was analyzed by HPLC (Shimadzu, CLASS VP model), in which a C-18 column was employed and a mobile phase of acetonitrile/water (60:40, v/v) with 1% acetic acid was used at a flow rate of 1.0 ml min^{-1}. An injection volume of 20 μl was used and the amount of TCP was determined by a UV detector.

3. Results and discussion

3.1. Physico-chemical characterization

The phase composition and the crystallite size of the prepared samples were examined by X-ray diffraction analysis. Fig. 1 presents the XRD patterns of calcined pure and iron doped TiO_2 (0.3, 0.5, 0.7 and 1 wt.%). The peaks obtained at various 2θ were identified by comparison with JCPDS Catalogue (no.21-1272) and confirmed that the particles are crystalline with an anatase structure. It is noteworthy that the diffractograms of all the samples do not present signals ascribed to the presence of doped metal. The absence of peaks due to metal may be attributed to fine dispersion of metal particles on TiO_2 or due to very small metal content. Doping of metals restricted the crystallite growth and reduced the size. Average crystallite size of TiO_2 was estimated according to the Scherrer's equation and the data are presented in Table 1.

From the diffused reflectance spectra shown in Fig. 2, it is obvious that the Fe–TiO_2 show photo absorption at 410–445 nm. On the other hand when the comparison is made between the UV–vis DRS of the Fe doped and undoped TiO_2, it is seen that the doping ions caused significant absorption shifts into visible region

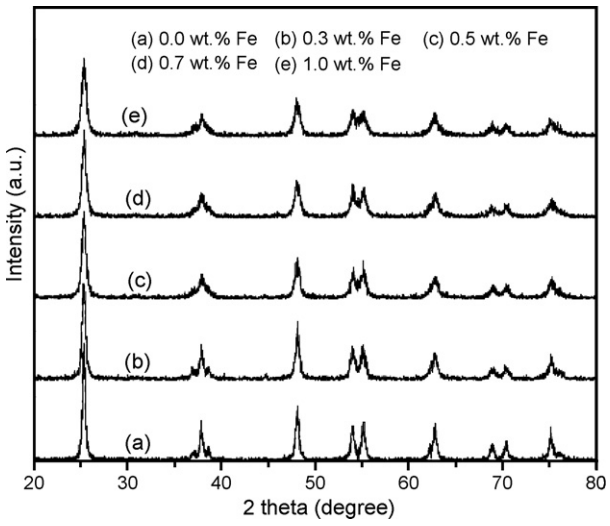

Fig. 1. X-ray diffraction patterns of TiO_2 and Fe–TiO_2.

Table 1
Physico-chemical properties of Fe–TiO_2

Fe–TiO_2	[a]Crystallite size (nm)	Band gap energy (eV)	Calculated *g* value	[b]Dopant concentration (wt.%)
0.0 wt.%	20.36	3.10	–	–
0.3 wt.%	17.89	3.02	1.999	0.215
0.5 wt.%	14.77	2.92	1.999	0.453
0.7 wt.%	12.65	2.84	(i) 2.000 and (ii) 4.20	0.615
1.0 wt.%	11.01	2.76	(i) 2.001 and (ii) 4.21	0.897

[a] XRD using Scherrer equation for anatase 1 0 1 plane.
[b] ICP-AES analysis.

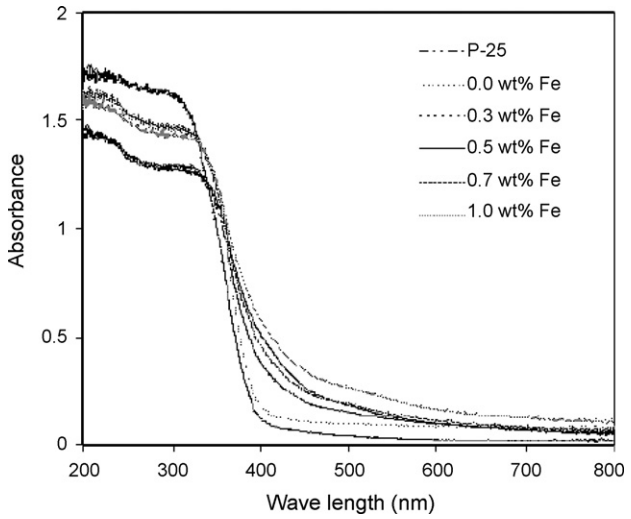

Fig. 2. UV–visible diffused reflectance spectra of TiO_2 and Fe–TiO_2.

compared to the absorption threshold of the pure TiO_2 and the band gap energy changes from 3.10 to 2.72 eV as loading level is increased. This observation strongly confirms the presence of metal on the titania matrix and the absence of detectable Fe oxide phase which are normally observed after 450 nm [13].

The EPR spectra of Fe–TiO_2 are shown in Fig. 3. The samples 0.3 wt.% Fe–TiO_2 (Fig. 3a) and 0.5 wt.% Fe–TiO_2 (Fig. 3b) are having a broad signal at $g = 1.999$ corresponding to Fe^{3+} in anatase lattice of TiO_2 and its intensity increases with increase in iron concentration. As the size of Fe^{3+} is less than Ti^{4+}, Fe^{3+} occupies sites vacated by Ti^{4+} in octahedral symmetry of anatase structure when calcined as reported in literature [14]. However, EPR spectra of the samples 0.7 wt.% Fe–TiO_2 (Fig. 3c) and 1.0 wt.% Fe–TiO_2 (Fig. 3d) show two signals at $g = 2.01$ and $g = 4.21$. The signal at

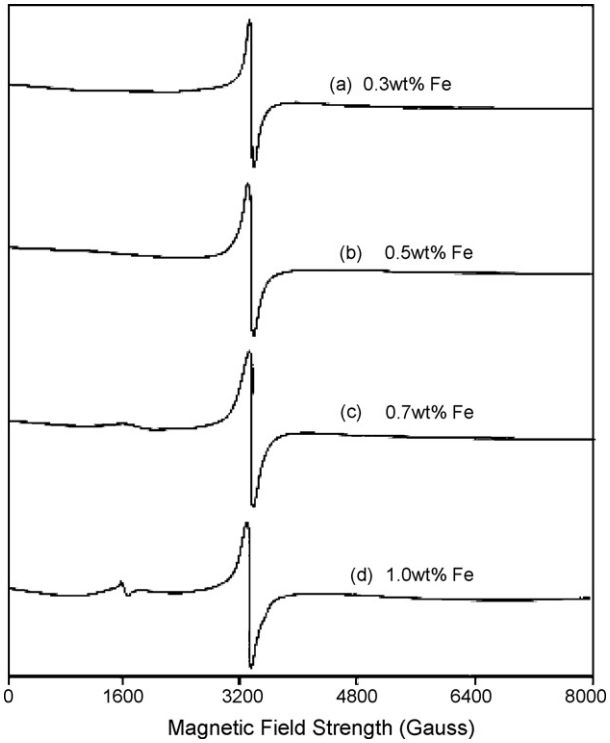

Fig. 3. Electron paramagnetic resonance spectra of Fe–TiO_2.

$g = 2.01$ is due to the presence of Fe^{3+} in anatase matrix as observed in samples 0.3 wt.% Fe–TiO_2 and 0.5 wt.% Fe–TiO_2. In addition to this the signal observed at $g = 4.21$ can be attributed to isolated high spin Fe^{3+} ions which are diffused to the surface of titania during heat treatment [15].

The TEM image of 0.5 wt.% Fe–TiO_2 nanoparticles are shown in Fig. 4a. The size of the most particles is within the range of 10–30 nm (Fig. 4b). Based on the available reports, it is understood that particle size ranging below 10 nm is not advantageous due to increase in band gap energy [16]. The inserted image in Fig. 4a shows the electron diffraction pattern of a single Fe–TiO_2 nanoparticle which confirms that the TiO_2 is in anatase phase.

3.2. Mineralization studies

The photodecomposition rate of pollutants is influenced by the photo absorption ability and the number of active sites of the catalyst used. The limitation of surface sites may control the decomposition rate at low dosage of semiconductor. High dose of the semiconductor will decrease the light penetration of the catalyst suspension and reduce the degradation rate.

In order to select optimum reaction parameters, the effect of concentration of 2,4,6-trichlorophenol and pH of the solution were investigated and found that when concentration of 2,4,6-trichlor-

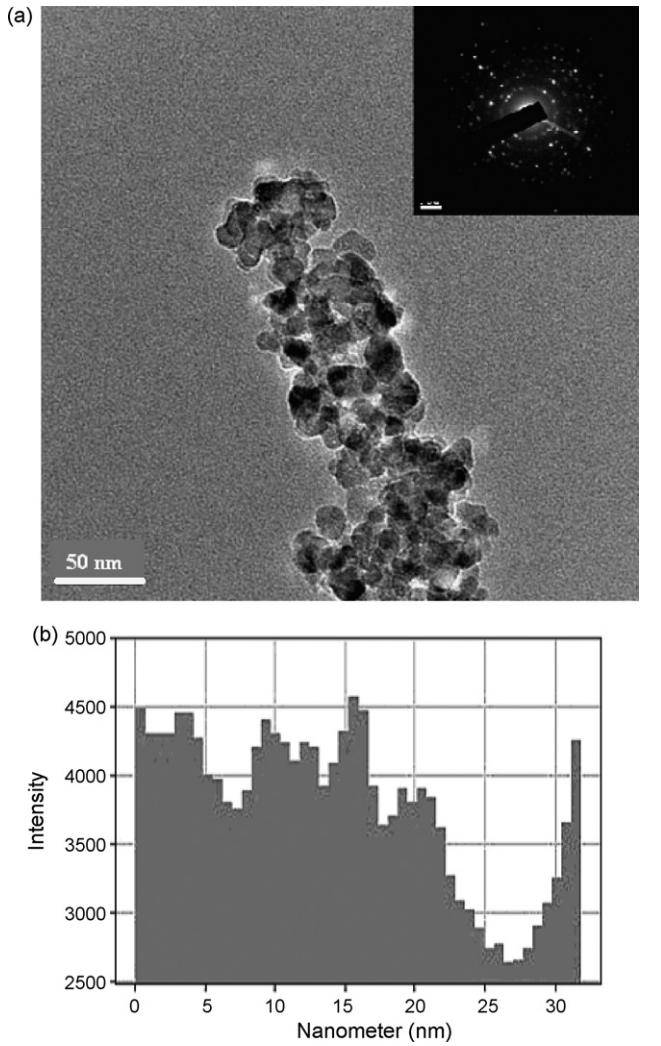

Fig. 4. (a) TEM image and ED pattern (insert) of 0.5 wt.% Fe–TiO_2 and (b) particle size distribution histogram of 0.5 wt.% Fe–TiO_2.

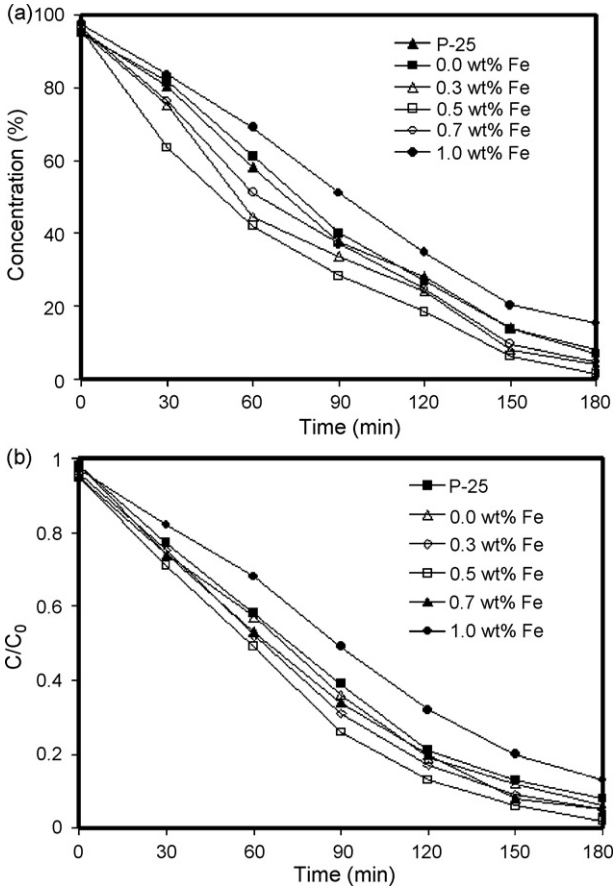

Fig. 5. (a) Degradation profiles and (b) mineralization profiles. Catalyst: Fe–TiO_2, catalyst dosage = 0.8 g/l, pH 5 and 2,4,6-TCP = 50 ppm.

ophenol is 50 ppm and when the pH is 5, the degradation rate is maximum. The maximum degradation of 2,4,6-trichlorophenol was observed with 0.8 g of Fe–TiO_2 per liter. Fig. 5a and b are degradation and mineralization profiles of 2,4,6-trichlorophenol with respect to time. It is evident that the degraded products are mineralized completely within the reaction time of 180 min.

3.2.1. *Influence of Fe doping on photocatalytic activity*

In order to attain optimum Fe dopant level, the target reaction was carried out on Fe–TiO_2 with dopant level of 0.3–1.0 wt.% and the results are presented in Fig. 6. The photo degradation efficiency of Fe–TiO_2 increased with increasing iron concentration, reaching a maximum at 0.5 wt.% Fe. The optimal amount of Fe on TiO_2 was found to be 0.5 wt.% as shown in Fig. 6. It is also seen that activity of 0.7 wt.% Fe–TiO_2 and 0.3 wt.% Fe–TiO_2 are higher than the bare TiO_2. However, when the photocatalytic activity of undoped TiO_2 and 1 wt.% Fe–TiO_2 are compared, undoped TiO_2 shows better catalytic activity than 1 wt.% Fe. It is reported that at low doping level of metal, photo generated holes and electrons are well separated thereby increasing the efficiency of the catalyst. Fe^{3+} traps photo generated holes and forms Fe^{4+} which will migrate to surface adsorbed hydroxyl ion to produce hydroxyl radicals and O^{2-} in the surface lattice of doped TiO_2 tends to trap photo-generated holes and produce hydroxyl radicals. Alternatively, Fe^{4+} may react with photogenerated electrons in which Fe^{3+} acts as recombination centre and thereby affecting the photocatalytic activity. All the interfacial charge transfer reactions involving Fe^{3+} occur only when Fe^{3+} ions are located close to the surface sites which is likely when the surface content of $Fe^{3+}$is appreciable. However at high doping level, there is considerable chance for multiple trapping which will reduce the efficiency of the photocatalyst [17]. Moreover, the detrimental activity at high iron loading may be due to the blocking core level semiconductor surface by Fe [18]. The introduction of transition metal resulted in the change of the electronic environment of TiO_2. A significant change in the particle size was noticed from XRD and TEM image of various catalysts. At the optimal loading of Fe doping, a greater percentage of iron particles are found to be in the range of 10–15 nm, which is beneficial for photo catalytic activity. Band gap energy is found to decrease as the doping concentration of Fe is increased. EPR results further confirm the fact that dopant metal exists in anatase matrix as Fe^{3+} both in 0.3 and 0.5 wt.% Fe–TiO_2. A reduction in particle size is also observed as Fe loading is increased. However, at 0.5 wt.% Fe, there is charge separation due to trapping of conduction band electron as seen from band gap energy value. Beyond 0.5 wt.%, both trapping of hole by dopant ion and blocking of core species i.e. titania from light harvesting by dopant ion are dominating and decreases the activity. Hence 0.5 wt.% Fe–TiO_2 was found to be a highly active photocatalyst.

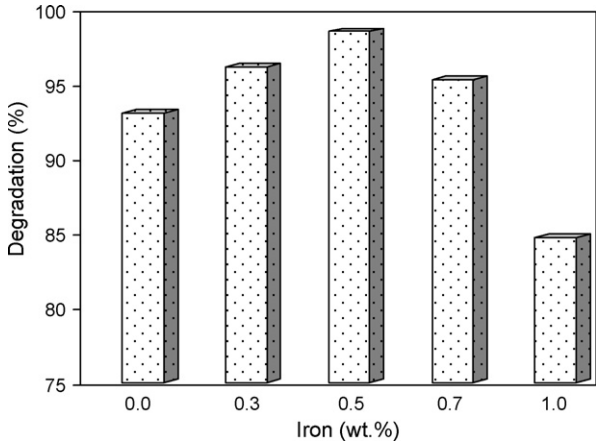

Fig. 6. Effect of iron concentration on degradation of 2,4,6-trichlorophenol. catalyst: Fe–TiO_2, catalyst dosage = 0.8 g/l, pH 5 and 2,4,6-TCP = 50 ppm.

4. Conclusion

Enhancement of the catalytic activity of TiO_2 has been achieved by doping Fe for photo catalytic degradation of 2,4,6-trichlorophenol. The driving force may be the separation of charge carriers. The doping of Fe caused significant absorption shift towards visible region compared to the Degussa P-25 and pure TiO_2. The photocatalytic activity has been found to depend on the band gap energy, nature of iron species and particle size. Active nanocrystalline Fe–TiO_2 (15 nm) found at the optimal Fe level of 0.5 wt.% was responsible for the photo catalytic oxidative degradation of 2,4,6-trichlorophenol. This study confirms the potential of heterogeneous photo catalyst to purify wastewater containing aromatic pollutants, particularly chlorinated substances, which are often toxic for microorganism in biological treatments.

References

[1] H. Roques, Chemical Water Treatment, VCH Verlag, Wienheim, Germany, 1996.
[2] M.R. Hoffmann, S.T. Martin, W. Choi, D.W. Bahnemann, Chem. Rev. 95 (1995) 69.
[3] E. Pelizzetti, N. Serpone (Eds.), Homogeneous and Heterogeneous Photocatalysis, Reidel Publishing Company, Dordrecht, 1986.
[4] A. Mills, R.H. Davies, D. Worsley, Chem. Soc. Rev. 22 (1993) 417.
[5] H. Chao, Y. Yun, H. Xingfang, L. Andre, Appl. Surf. Sci. 200 (2002) 239.
[6] S. Rengaraj, X.Z. Li, J. Mol. Catal. A: Chem. 243 (2006) 60.

[7] M.A. Barakat, H. Schaeffer, G. Hayes, S. Ismat Shah, Appl. Catal. B: Environ. 57 (2005) 23.
[8] T. Essam, M.A. Amin, O.E. Tayeb, B. Mattiasson, B. Guieysse, Chemosphere 66 (2007) 2201.
[9] I.J. Ochuma, R.P. Fishwick, J. Wood, J.M. Winterbottom, J. Hazard. Mater. 144 (2007) 627.
[10] S. Anandan, A. Vinu, T. Mori, N. Gokulakrishnan, P. Srinivasu, V. Murugesan, K. Ariga, Catal. Commun. 8 (2007) 1377.
[11] T. Lopez, R. Gomez, G. Pecci, P. Reyes, X. Bokhmi, O. Novaro, Mater. Lett. 40 (1999) 59.
[12] H. Kominami, J. Kato, Y. Takada, Y. Doushi, B. Ohtani, S. Nishimoto, M. Inoue, T. Inui, Y. Kera, Catal. Lett. 46 (1997) 235.
[13] E.P. Reddy, L. Davydov, P.G. Smirniotis, J. Phys. Chem.: B 106 (2002) 3394.
[14] E. Abi Aad, A. Aboukaıs, Catal. Today 56 (2000) 371.
[15] R. Janes, L.J. Knightley, C.J. Harding, Dyes Pigments 62 (2004) 199.
[16] H. Lin, C.P. Huang, W. Li, C. Ni, S. Ismat Shah, Y.H. Tseng, Appl. Catal. B: Environ. 68 (2006) 1.
[17] J. Zhu, W. Zhang, B. He, J. Zhang, M. Anpo, J. Huang, L. Zhang, J. Mol. Catal. A: Chem. 216 (2004) 35.
[18] K.T. Ranjit, B. Viswanathan, J. Photochem. Photobiol. A: Chem. 108 (1997) 79.